J Mater Sci (2019) 54:3694–3709

Ceramics

Characterization of grain boundary disconnections in $SrTiO_3$ part I: the dislocation component of grain boundary disconnections

Hadas Sternlicht[1], Wolfgang Rheinheimer[2], Rafal E. Dunin-Borkowski[3], Michael J. Hoffmann[4], and Wayne D. Kaplan[5,*]

[1] School of Engineering, Brown University, Providence, USA
[2] Materials Engineering, Purdue University, West Lafayette, USA
[3] Ernst Ruska-Centre for Microscopy and Spectroscopy with Electrons and Peter Grünberg Institute, Forschungszentrum Jülich GmbH, Jülich, Germany
[4] Institute of Applied Materials, Karlsruhe Institute of Technology, Karlsruhe, Germany
[5] Department of Materials Science and Engineering, Technion – Israel Institute of Technology, Haifa, Israel

Received: 18 September 2018
Accepted: 30 October 2018
Published online: 15 November 2018

ABSTRACT

High-resolution transmission electron microscopy is often used to characterize grain boundaries, but it is usually limited to special high symmetry boundaries with a high density of coincident sites. For these 'special' boundaries, both crystals can be brought into a low-index zone-axis with the boundary plane parallel to the incident electron beam. In this case the atomistic structure of the boundary can be solved, which is not possible for other, more general grain boundaries. In the present study, *general* grain boundaries in $SrTiO_3$ were analyzed using aberration-corrected transmission electron microscopy and scanning transmission electron microscopy. These boundaries included at least one type of disconnection (i.e., defects that can have a step and/or a dislocation component). Since the dislocation component of disconnections along general grain boundaries cannot be fully resolved using the methods currently available, a plane matching approach was used to compare disconnections at different boundaries. Using this approach, the dislocation component of the disconnections was partially characterized and was found to have an edge component mainly parallel to {100} and {110}, close to normal to the macroscopic grain boundary plane. The step component of the disconnections was found to be aligned mainly parallel to the same crystallographic planes ({100} and {110}).

Hadas Sternlicht: Conducted when the author was at Department of Materials Science and Engineering, Technion—Israel Institute of Technology, Haifa Israel.
Wolfgang Rheinheimer: Conducted when the author was at Institute of Applied Materials, Karlsruhe Institute of Technology, Karlsruhe, Germany.

Address correspondence to E-mail: kaplan@technion.ac.il

https://doi.org/10.1007/s10853-018-3096-4

Introduction

Grain boundary migration is a well-known phenomenon and a fundamental process in microstructural evolution. One of the models that was suggested to describe the mechanism of grain boundary motion is the terrace-ledge-kink (TLK) model [1, 2]. According to this model, the process of grain boundary migration occurs through diffusion of atoms from the grain boundary plane (analogous to a surface terrace), then to a step site, and finally to a kink site. The concept of steps at grain boundaries has been evaluated, and 'disconnections' were defined which are defects at grain boundaries which can have a step and/or a dislocation character [3]. Pond et al. postulated that disconnections play a key role in the atomistic mechanism of grain boundary migration [3–10]. For a recent review of the theory of disconnection kinetics, see [11].

Recently, steps were found at general grain boundaries in $SrTiO_3$ [12] and were correlated with the mechanism of grain growth following the TLK and disconnection models [1–10]. It was shown that the steps consistently appeared along grain boundaries in samples annealed under both high and low oxygen partial pressures [12]. In samples annealed under a relatively high oxygen partial pressure, the step and grain boundary planes were mainly parallel to {100} and {110} planes, regardless of the annealing temperature, the cooling rate, or the orientation of the grains creating the boundary. Accordingly, the step free energy is anisotropic. Since these steps do not start and end at atomic positions which coincide in both grains, these steps also include a dislocation component, creating disconnections [5, 6, 9, 13, 14].

According to the disconnection model, a step separates two identical segments of a boundary plane which are energetically degenerate (have the same energy), where in a demi step the equivalent boundary planes (which are energetically degenerate) are separated by a point symmetry operation. Whenever a step separates distinct boundary planes, it is defined as an imperfect defect, labeled as a partial step [3]. In addition, a disconnection is defined as perfect when separating regions of the grain boundary plane which are energetically degenerate and is defined as partial when separating regions of the boundary plane which are not energetically degenerate [6]. In addition to disconnections, secondary grain boundary dislocations were defined in the past [13, 14] as dislocations which could be smaller than a lattice dislocation.

In the present work, the structure of disconnections at general grain boundaries in $SrTiO_3$ which was annealed under a relatively high partial pressure of oxygen (pure oxygen or air) was characterized. Aberration-corrected transmission electron microscopy (TEM) was used to discern the dislocation component of the disconnections. General grain boundaries were studied in the form of either polycrystalline $SrTiO_3$ or boundaries between a single crystal of $SrTiO_3$ of a predefined orientation diffusion-bonded to polycrystalline $SrTiO_3$. The boundaries were characterized using the available methodologies for defining the Burgers vectors of the defects, and the limitations of these methods restricted full characterization of the dislocations (see supplementary material). Since available methodologies can't be used to characterize dislocations at general grain boundaries, a plane matching approach was used in this work to partially characterize the dislocation component of the disconnections in each of the studied boundaries. It should be noted that $SrTiO_3$ was selected due to its rather simple perovskite structure. However, the methods used here could be applied to grain boundaries in other materials as well.

The kinetics of grain boundary motion of $SrTiO_3$ annealed under a relatively high partial pressure of oxygen was studied by Rheinheimer et al. A significant decrease in the grain boundary mobility was found with increasing temperatures between 1350 °C and 1425 °C [15, 16]. Since the physical origin of this counterintuitive behavior is not yet known, the present work focused on samples annealed in this temperature range to reveal a possible correlation between the grain boundary defect structure and the decrease in the grain boundary mobility.

Experimental methods

$SrTiO_3$ samples

Stoichiometric polycrystalline $SrTiO_3$ powder was prepared by a mixed oxide/carbonate route using $SrCO_3$ (99.95%, Sigma-Aldrich Chemie GmbH, Taufkirchen, Germany) and TiO_2 (99.995%, Sigma-Aldrich). Powder was pressed uniaxially and

isostatically (400 MPa) to form cylindrical green bodies (14 mm diameter, 6 mm height). The green bodies were sintered at 1425 °C for 1 h in oxygen (as sintering is significantly faster than grain growth at this temperature) to a relative density of 99.5 ± 0.2% and a mean grain size of ~1 μm. Further details of sample preparation methods are published elsewhere [17].

Two different types of samples were used: standard polycrystalline bulk samples and diffusion-bonded samples as used in the seeded polycrystal technique [16]. The polycrystalline matrix needed for diffusion-bonded samples was cut into disks and polished (diamond slurry, 0,25 μm). The $SrTiO_3$ single crystals (impurity content: <10 ppm Si, <2 ppm Ba, <1 ppm Ca, SurfaceNet GmbH, Rheine, Germany) were chemically–mechanically polished and placed between two polished polycrystalline disks. The samples were heated to 1430 °C for 20 min in air with a load of 1 MPa to bond the single crystals to the polycrystals. Two surface orientations of the single crystals were used, i.e., {100} and {110}. This method was described in detail elsewhere [16].

For all growth experiments, tubular furnaces were used (Gero GmbH, Neuhausen, Germany) at temperatures between 1350 °C and 1550 °C. Either pure oxygen or air was used as atmospheres at ambient pressure. The heating rate was 20 K/min.

Two different cooling methods were used to maintain conservation of the high-temperature boundary structure for subsequent TEM observations. Samples were either removed from the hot zone of the furnace (referred to as gas quenching in the following) or quenched in water. For gas quenching an initial cooling rate of ~200 K/min was measured by an uncovered thermocouple located close to the sample. Water quenching was done without changing the atmosphere and resulted in cooling to below 100 °C within 3 s due to the small sample volume (5 × 5 × 3 mm^3). A detailed overview of the samples used in the present study is listed in Table 1.

Characterization methods

The bulk samples were characterized using an aberration-corrected TEM (FEI Titan 80–300 keV S/TEM) operated at 300 keV and an FEI Titan 50-300 PICO (Figs. 1 and 2 in the present manuscript and Figs. S1 and S2 in the supplementary material) operated at 200 keV [18]. TEM samples were prepared using the following methods:

(a) The conventional approach based on diamond slicing, mechanical thinning, mechanical dimpling, and ion milling with Ar at 2-5 kV, for polycrystalline samples.
(b) The lift-out technique using a dual-beam focused ion beam (FIB; FEI Strata 400 s) for selecting and preparing TEM samples from specific boundaries between the single crystal and a grain from the polycrystalline side of diffusion-bonded samples [19].

Each boundary was tilted to reach the "edge-on" condition, in which the electron beam is parallel to the grain boundary and step planes (defined in [12]). Each of the studied boundaries was randomly selected.

One conventionally prepared TEM specimen (from a polycrystalline bulk sample that was sintered at 1425 °C for 1 h in oxygen, annealed at 1350 °C for 10 h in oxygen and furnace-cooled), was re-annealed in air at 900 °C for 2 h, as a TEM specimen.

Results

General grain boundaries in $SrTiO_3$ were characterized using high-resolution TEM (HRTEM) and high-angle annular dark field scanning TEM (HAADF STEM). When orienting these boundaries to the edge-on condition, disconnections composed of nanometric steps and dislocations were detected along the boundaries. The steps were of the same nature as previously reported [12], parallel mainly to {110} and {100} planes.

Case set 1: One general grain boundary for which the atomistic structure can be determined

Dislocations were characterized in a boundary from a sample in which a (100) single crystal of $SrTiO_3$ was diffusion-bonded to polycrystalline $SrTiO_3$. The sample was annealed at 1425 °C for 10 h in oxygen and water-quenched. A HAADF STEM micrograph of a boundary between the single crystal and a grain from one of the polycrystalline parts of the sample is presented in Fig. 1. While the boundary is edge-on and the grain on the right side of the micrograph

Table 1 An overview of the samples used in the present study

Sample type	Annealing temperature (°C)	Cooling method
Polycrystalline	1350	Furnace-cooled
	1550	
	1350	Gas-quenched
		Water-quenched
Diffusion-bonded	1425	Water-quenched
	1350	

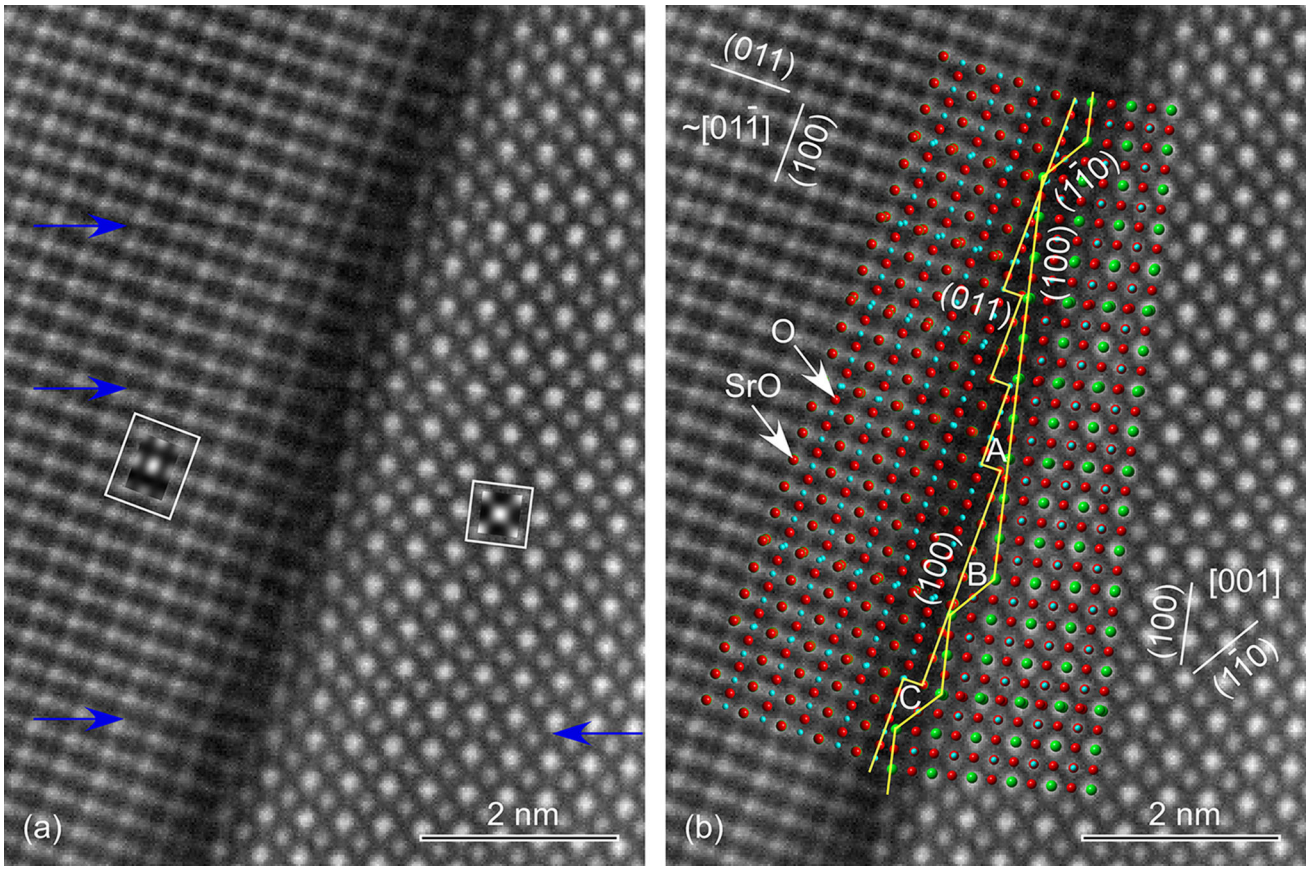

Figure 1 **a** HAADF STEM micrograph of an edge-on grain boundary. The grain on the left is close to a [01$\bar{1}$] zone-axis, and the right grain is in the [001] zone-axis. The micrograph was filtered to remove noise (average background subtraction). The arrows indicate examples for distortions originating from the HAADF STEM data acquisition. The insets present QSTEM simulations of the image in both grains. **b** The HAADF STEM micrograph in (**a**) with the atomistic model. Nanometer length-scale steps are visible along the boundary (marked in yellow). In the atomistic solution green circles represent Sr, red circles represent O, and blue circles represent Ti.

(which is the single crystal) is in the [001] zone-axis, the grain on the left side slightly deviates from the [01$\bar{1}$] zone-axis. This deviation from the [01$\bar{1}$] zone-axis is identified by the slightly distorted unit cell of this grain. While the conditions normally required to determine the atomistic structure of a grain boundary are not met, the slight deviation from a low-index zone-axis for the grain on the left is assumed to be minor in the following, and the data are used to develop an atomistic model.

To find the atom positions in the STEM micrograph in Fig. 1a, simulations were performed using QSTEM (see supplementary material) [20]. The simulations were prepared using a convergence angle of 29.9m-rad, a source size of 0.07 nm, accelerating voltage of 200 kV, Cs=1 mm, and a detector with inner and

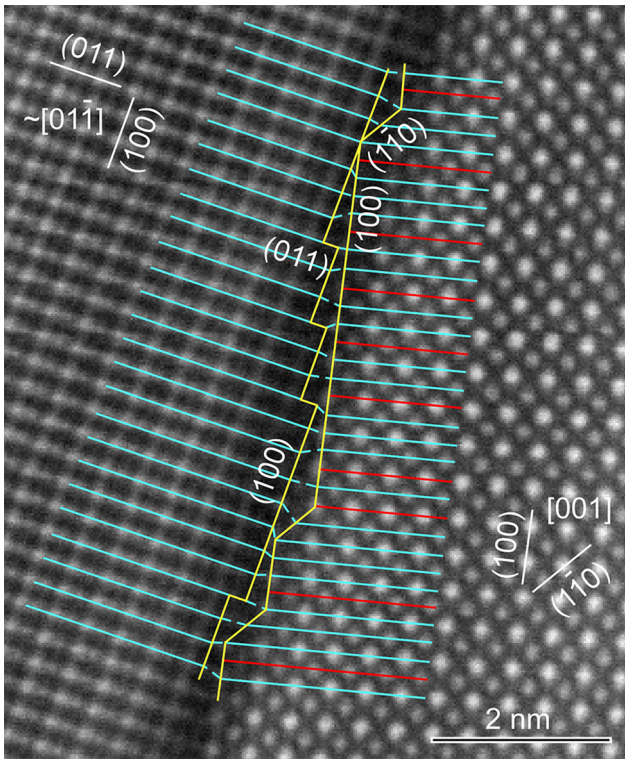

Figure 2 Dislocation analysis of the boundary presented in Fig. 1. Lines along dense planes which lie within a small as possible angle from the boundary plane normal were drawn to account for the projection of the close-to-normal edge component of the dislocations along the boundary.

outer collection angles of 80–200 mrad. In Fig. 1a simulations of both delimiting grains with a thickness of about 30 nm are presented in the insets (as detailed in the supplementary material). Based on the simulations presented in the insets in each of the grains, heavy atoms appear with bright contrast in the image and oxygen atoms are not detected. Based on the simulation, the atoms positions are presented in Fig. 1b.

While the macroscopic grain boundary plane can be defined based on the experimental data in Fig. 1, the main points of interest in this work are the microscopic degrees of freedom, which define the crystallographic planes parallel to the steps and flat grain boundary plane segments. From close inspection of the lattice structure of both grains at the boundary region in Fig. 1a, the steps and grain boundary planes can be defined using the terminating crystallographic planes of each delimiting grains (yellow lines in Fig. 1b). However, this leaves a region at the core of the boundary which has a symmetry different from each of the delimiting crystals (between the yellow lines marked in both grains), indicating the diffuse nature of the grain boundary core [21]. In this study, disconnections are associated with the mechanism of grain boundary motion, so we focus on the nature of the steps and the grain boundary dislocations associated with them.

In addition to sample drift and charging, the misorientation of the left grain in Fig. 1a from a low-index zone-axis adds additional error in determination of the atomic column positions. As a result, there is an intrinsic uncertainty in defining the positions of columns of atoms. This error was estimated by overlaying the ideal unit cell on the micrograph, illustrating regions of deviation which are marked in Fig. 1b, in addition to the arrows marked in Fig. 1a demonstrating examples of distortions in the acquired data. Since the overall deviations are small ($\sim$0.5Å), changes in atomic column positions due to strain, reconstruction or relaxation cannot be separated from the STEM distortions. Thus, small changes in the atom positions are ignored (as in Figs. S1 and S2).

It should be noted that the boundary plane in Fig. 1 appears dark in the HAADF STEM micrograph. This was also noted in other boundaries characterized using STEM, in which electron energy loss spectroscopy (EELS) thickness maps confirmed that this effect is not caused by a change in the thickness of the sample. This dark appearance of the boundary can be attributed to kinematic and dynamic scattering resulting from de-channeling of the electron beam due to the difference in structure of the boundary compared to the bulk grains. In addition, diffuse scattering, such as thermal diffuse scattering [22] and Huang scattering [23], will also result in dark appearance of the boundary. Huang scattering arises from local shifts in some atom positions. While Huang scattering originally refers to shifts in positions in the vicinity of solute atoms, grain boundaries have weaker bonding than the bulk, resulting in different phonon modes [23]. In addition, the atomistic structure at the core of dislocations is modified from the bulk structure, potentially contributing to diffuse scattering in the vicinity of the boundary planes, indicating the potential presence of grain boundary dislocations in the boundary shown in Fig. 1. As will be shown below, dislocations are present along the boundary contributing to the dark contrast in HAADF mode [24]. The dark appearance of the boundary may also occur due to strain along

the boundary, in part contributed from dislocations (which are characterized below and in the supplementary material). Chemical analysis of the boundary indicates that the boundary is slightly non-stoichiometric (the details of which will be published separately). The non-stoichiometry of the boundary may also contribute to its dark appearance, since slight changes in the atomistic structure at the boundary area will occur due to changes in stoichiometry, adding to Huang scattering, in addition to changes in the density (and thus of the Z number which strongly affect the contrast in HAADF STEM micrographs) and to the de-channeling of the electron beam. Dark contrast in HAADF micrographs and in dark field STEM of the boundary region was also noted in other studies on $SrTiO_3$ [25–28].

It should be considered that some signal is apparent in the regions between the disconnections in the darker region along the boundary (between the yellow lines along both grains in Fig. 1b), which should be free of atoms according to the simplistic atomistic solution. This contrast is attributed to steps along the thickness of the TEM sample (defined as "inclined steps"), which shift the position of the grain boundary plane between the two grains along the TEM sample thickness [29]. Thus, the position of the step and grain boundary planes changes along the projected thickness of the sample as discussed in [29]. In addition, chemical analysis of the boundary indicates that the boundary is slightly non-stoichiometric, and the contrast in these regions could be due to chemical excess. An additional option could be that these regions are occupied by dislocation cores which are expected to appear along the boundary. Dislocation cores along grain boundaries in $SrTiO_3$ were previously shown to deviate from the stoichiometric composition, contributing to a detectable signal in the dark regions of the micrograph [30].

Types of grain boundary disconnections

Two types of disconnections were detected along the boundary shown in Fig. 1. One type includes both a dislocation and a step component and can be found whenever a step is present along the boundary in one of the grains. This type of disconnection also has a dislocation component since these steps do not start and end at atomic positions which coincide in both grains. This type of disconnection can be composed of either a step from the grain on the left and a grain boundary plane from the grain on the right (for which s, the step vector, is 0. An example is marked as A in Fig. 1b), a grain boundary plane from the grain on the left and a step from the grain on the right (an example is marked as B in Fig. 1), or steps from both grains with varying translations between the two (an example is marked as C in Fig. 1b). The second type of disconnection includes only a dislocation component, which are in effect grain boundary dislocations resulting from the orientation mismatch between the two grains. Both types of disconnections are not uniform along the boundary due to the low symmetry of the boundary and perhaps due to the transitory morphology of the boundary due to its motion.

It should be noted that in Fig. 1 the steps on the grain on the left are partial steps and those on the grain on the right are (full) steps (rather than demi steps). The disconnections are both partial and perfect disconnections. In this case, when a disconnection is composed of a step from the grain on the right and a grain boundary plane from the grain on the left (defined as B in Fig. 1b), a perfect disconnection is formed. This is the result of a step which separates two regions of the grain boundary plane of the grain on the right, which are energetically degenerate. It should be noted that the definition of a perfect disconnection takes into account the sum of the surface energies when considering the grain boundary energy and ignores the interactions between atoms along the grain boundary. In Fig. 1, the positions of the atoms along the boundary with respect to both delimiting grains are different when considering two sections of the boundary divided by a step from the grain on the right. This results in different interactions between the atoms across the boundary at the two sides of the step and a modification of the grain boundary energy. As such, the grain boundary energies on both sides of the step will be slightly different, defining a local driving force for step motion. Only when ignoring the interactions between atoms, the sections of the grain boundary created from both sides of the step are degenerated. When considering a disconnection which is composed of a step from the grain on the left and a grain boundary plane from the grain on the right (defined as A in Fig. 1b), or disconnections which are composed of steps from both grains with varying distances (defined as C in Fig. 1b), partial disconnections are formed as the interfacial states separated by the steps

are not degenerated. The grain boundary dislocations are also a type of partial disconnections. The supplementary material demonstrates that the available methods for characterizing the dislocation component of disconnections at general grain boundaries fail in the case of general grain boundaries, as the boundary demonstrated in Fig. 1.

Case set 2: General grain boundaries where the atomistic structure cannot be determined

While a model for the atomistic structure of the specific general grain boundary presented in Fig. 1b could be determined from the experimental data, this is not the case for most *general* high-angle grain boundaries. For most general high-angle grain boundaries, where the grain boundary and step planes are aligned to edge-on condition, at least one grain is not in a low-index zone-axis. As such, the atomistic structure of the boundary cannot be determined from established electron microscopy techniques, and the dislocation character of the disconnections cannot be found. In addition, since the density of the dislocations along general high-angle boundaries is high (as demonstrated for the boundary in case set 1 in the supplementary material), individual dislocations often can't be resolved. Thus, to characterize the dislocation component of the disconnections, a geometric approach was used where the edge component of a dislocation which is close to normal to the boundary was related to the appearance of extra planes in one of the grains.

In this approach, high-density planes in one grain, which are oriented at a small as possible angle from the boundary plane normal, were correlated with high-density planes oriented at a small as possible angle from the boundary plane normal in the second grain. Extra crystallographic planes in one of the grains, which have no matching planes in the other grain, can be determined. By using this method, we assume that dislocations have a component projected along dense planes, as was previously reported to occur in $SrTiO_3$ [31–33]. It should be noted that in such a manner only the projection of the edge component of the dislocations which is close to normal to the boundary is characterized (and a screw component is expected as discussed in the supplementary material for the boundary in case set 1).

Along the boundaries, varying displacements between planes of atoms from the grains defining the boundary are visible (see, for example, light blue lines in Fig. 2). These displacements can be treated as a set of grain boundary dislocations (a type of disconnections which only have a dislocation character) accommodating the second type of disconnections (which have both a step and a dislocation character), and the mismatch between the grains, as discussed in Case Set 1 and the supplementary material. Since we cannot separate one dislocation from another due to their high density and since the atomistic solution of the boundary is not available in most cases, all of these displacements were summed and expressed here by the number of extra planes along a microscopic grain boundary plane segment (between steps) in one of the grains.

Since a TEM micrograph is a 2-D projection of a 3-D object, the edge component of the dislocation component of the disconnections yields a projection of the dislocations in the system, where the position of the dislocation along the thickness of the TEM specimen is not fully discerned. In addition, "inclined steps", or disconnections which are not edge-on and are located along the electron beam direction in the TEM specimen, also contribute to ambiguity in analysis of the dislocation nature [29]. Thus, it is not possible to accurately determine whether these are pure edge dislocations or whether they have a screw component. We assume that in general grain boundaries the dislocation component of the disconnections has both edge and screw components. However, based on the result presented here (as will be described below for Figs. 2, 3, 4, 5, and 6), the dislocations will necessarily have a component in dense directions (such as <100> and <110>) close to normal to the boundary. Thus, the resulting extra planes describe the 2-D projection of the sum of the edge component of the dislocations close to normal to the boundary between two such extra planes. The direction which is close to normal to the boundary was selected for simplicity. At the same time, a direction which is close to parallel to the boundary can be selected. However, this direction is harder to track due to the low symmetry exhibited in general boundaries.

Due to the inability to solve the full atomistic structure of the boundaries in the general case, bright spots in TEM micrographs were assumed to define atomic columns. This assumption was made since all

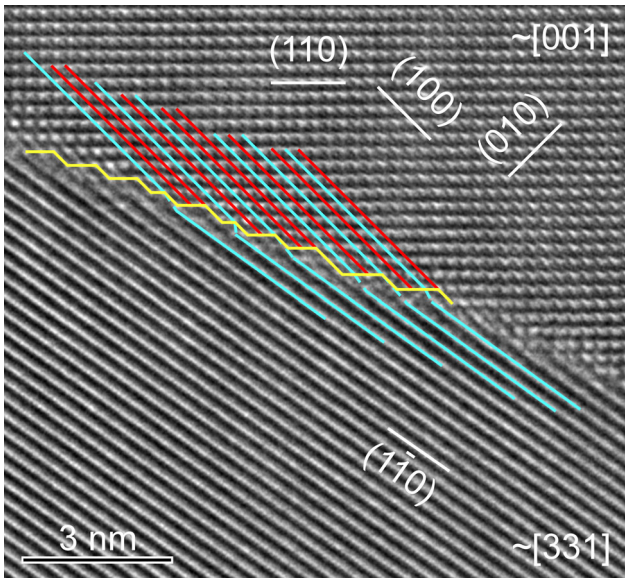

Figure 3 HRTEM micrograph of an edge-on general grain boundary. The upper grain is close to a [001] zone-axis. Nanometer length-scale steps are visible along the boundary (marked in yellow). The lower grain is close to a [331] zone-axis. In the upper grain (010) could have been used for the analysis. (100) planes were used to simplify the presentation. Both (100) and (010) will give the same result. Extra planes are marked along the boundary in red. The micrograph was acquired using a Cs of − 5.69 µm and Wiener-filtered to remove noise (reproduced with permission from [12]).

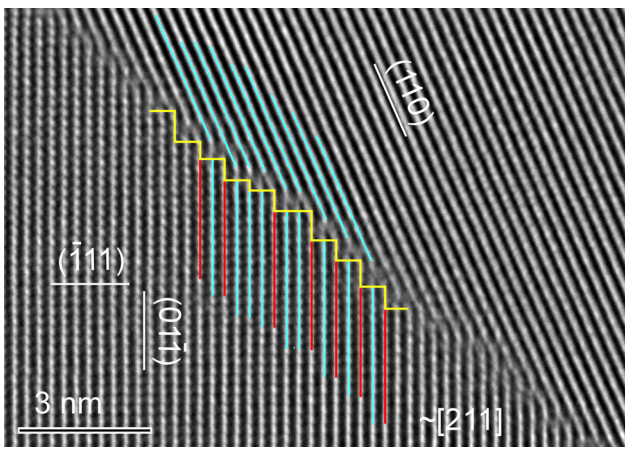

Figure 4 HRTEM micrograph of an edge-on grain boundary. The lower grain is oriented close to a [211] zone-axis. Nanometer length-scale steps are visible along the boundary (marked in yellow). Extra planes are marked along the boundary in red. The micrograph was acquired using a Cs=− 6.8 µm and Wiener-filtered to remove noise (reproduced with permission from [12]).

micrographs were acquired close to negative Cs conditions which results in bright contrast associated with atomic column positions [34].

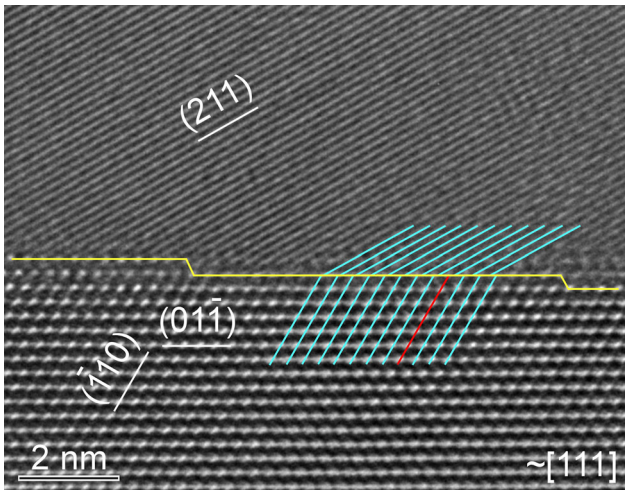

Figure 5 HRTEM micrograph of an edge-on grain boundary. The lower grain is close to a [111] zone-axis. Nanometer length-scale steps are visible along the boundary. Extra planes are marked along the boundary in red. The micrograph was acquired using a Cs=− 7.0 µm and Wiener-filtered to remove noise (reproduced with permission from [12]).

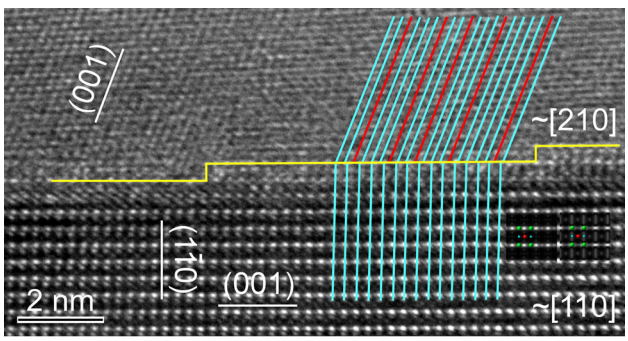

Figure 6 HRTEM micrograph of an edge-on grain boundary. The lower grain is close to a [110] zone-axis. The upper grain is close to a [210] zone-axis. Nanometer length-scale steps are visible along the boundary. Extra planes are marked along the boundary in red. The micrograph was acquired using a Cs=− 7.0 µm and Wiener-filtered to remove noise. In the atomistic solutions green represents Sr, red O, and blue Ti (reproduced with permission from [12]).

As an example, the above-mentioned approach was applied to the boundary presented in Fig. 1, as depicted in Fig. 2. Every plane of atoms from the left grain was defined as correlated with a plane of atoms from the right grain (both are marked in light blue). Every two or three planes of atoms there is an extra plane on the right grain, which is the projection of the sum of the edge components of dislocations which are close to normal to the boundary. It should be noted that in the single crystal which is oriented in

the [001] zone-axis, the (200) planes were used (rather than only (100) planes) as both (100) and (200) planes are high-density planes.

A second sample that was characterized was a polycrystalline sample that was annealed at 1350 °C for 10 h in oxygen and furnace-cooled. A HRTEM micrograph of an edge-on grain boundary from this sample is presented in Fig. 3. When correlating planes of atoms from the upper grain with planes of atoms from the lower grain (marked in light blue), there are one or two extra planes in the upper grain (marked in red) every second plane. As explained above, in the upper grain which is oriented close to the [001] zone-axis, (200) planes were used. Therefore, along the boundary, one or two extra planes are visible along each grain boundary plane segment.

The dislocations in Fig. 3 appear as extra (200) planes in the upper grain, which is oriented close to a low-angle zone-axis ([001]), yielding either extra Sr-O planes or TiO-O planes. The extra planes which account for the dislocations originate from $(1\bar{1}0)$ planes in the lower grain. The full structure of the boundary could not be derived from the experimental data, due to the deviation from a low-index zone-axis in both grains, which results in multiple atomistic solutions with poor fitting between the experimental micrograph and simulations.

Another polycrystalline sample, annealed at 1350 °C for 10 h in oxygen, and quenched in gas at a cooling rate of ~200 °C/min, contained one extra plane along each grain boundary plane segment (Fig. 4). The close-to-normal edge component of the dislocations was characterized as extra $(01\bar{1})$ planes in the grain which was oriented close to a [211] zone-axis, originating from (110) planes in the grain which is far from a low-index zone-axis (Fig. 4).

A sample similar to that shown in Fig. 4 was further annealed at 1350 °C in air and quenched in water. Barely any extra planes along each grain boundary plane segment are visible (Fig. 5). The close-to-normal edge component of the dislocations is characterized as extra $(\bar{1}10)$ planes of the grain which is close to a [111] zone-axis, originating from (211) planes in the grain which is not oriented close to a low-index zone-axis.

A second boundary from this sample is presented in Fig. 6. In this case, extra planes are present along each grain boundary plane segment. The edge component of the dislocations which is close to normal to the boundary is characterized as extra planes parallel to (001) planes of the grain which is oriented farther away from a low-index zone-axis ([210]), originating from $(1\bar{1}0)$ planes of the grain which is closer to a low-index zone-axis ([110]).

Since both grains are not in a low-index zone-axis, the full atomistic structure of the boundary cannot be determined. Two HRTEM simulations are presented in the insets in Fig. 6. The one on the left presents a simulation of $SrTiO_3$ in the [110] zone-axis with a thickness of 8.98 nm and an objective lens focus of − 21 nm (Cs=− 7.0 μm as in the experimental micrograph). In this solution the SrO columns are not represented by the brightest spots in the micrograph. The inset on the right presents the same simulation with a thickness of 9.77 nm and focus of 18 nm. In this solution the SrO columns are represented by the brightest spots in the micrograph. Both of these simulations and others present good fitting with the experimental micrograph. Due to the tilt of the lower grain from the [110] zone-axis, multiple solutions between simulated images and the experimental micrograph were found. Since they offer different atomistic solutions, a single solution for the atomistic structure of the boundary could not be found.

Discussion

Eighteen general grain boundaries in total were characterized as described above to account for dislocations along the boundaries from all the samples that are listed in Table 1, as well as a TEM sample from polycrystalline $SrTiO_3$ which was annealed at 900 °C in air. In samples annealed under a relatively high oxygen partial pressure at different temperatures and cooled at different cooling rates (furnace-cooled, gas-quenched, and water-quenched), two types of disconnections were detected. While we can divide these disconnections by the existence or lack of existence of a step component, these two types of disconnections can appear in practice in the form of a variety of different disconnections. One can find disconnections without a step component (grain boundary dislocations), disconnections composed of a step in one grain and a grain boundary plane on the other grain or steps in both grains with varying shifts between them. As such, a variety of possible dislocation components of disconnections are expected.

Dislocations at grain boundaries and their relation to the mechanism of grain boundary motion

Recently, the mechanism of grain boundary motion was correlated to the presence of disconnections at general grain boundaries in $SrTiO_3$ [12]. The motion of the macroscopic grain boundary plane is thus facilitated by the motion of the disconnections along the boundary. While the results presented here (and in [12]) were acquired ex situ, in situ experiments confirming these findings were done and will be published separately. The movement of these disconnections requires motion of both the steps and the dislocation components. The motion of the step character requires mass transport, where the motion of the dislocation component can be by climb and glide.

Since the characterization of the disconnections in this work was conducted by TEM, i.e., by 2-D projections of the bulk material, the direction of dislocation glide was not discernible. We consider that the active sites during the motion of the disconnections are kink sites. The motion of a step is visible in the TEM by its movement along the grain boundary plane, which requires the motion of a kink perpendicular to it. Once a kink has moved along a certain length of a step, the step in this region will move perpendicular to the motion of the kink, along the grain boundary plane.

Hirth and Pond conducted a detailed analysis to account for the motion of the disconnections along grain boundaries [3]. They defined the overlap step height as the overlapping distance between the steps in each grain, each multiplied by a unit vector normal to the grain boundary plane pointing to one of the grains (the λ grain, as defined in the supplementary material, where both are expressed in the coordinate system of the λ grain), and the normal component of the Burgers vector (normal to the grain boundary plane) as the difference between these expressions. They proposed that the overlap step height, the normal component of the Burgers vector, the densities of the atoms in the two grains, and the length of the disconnection in the relevant direction (in the grain boundary plane perpendicular to the motion direction) are related to the amount of material transferred (by substitutional atoms) from one grain to the other once the disconnection moves along the grain boundary plane. Artificially, the flux of material related to the motion of the dislocation component is defined by the normal component of the dislocation associated with the growth of one of the grains without transfer of material, where the motion of the step is related to material transfer between the grains, and depends on the overlap step height and on the densities of the two grains. In practice, the dislocation and the step characters move together. Motion by glide will occur when the number of atoms of each species that diffuse when the disconnection moves is zero (where the Burgers vector shouldn't necessarily be parallel to the grain boundary plane), otherwise long-range diffusion must occur, and motion by climb is required. Lateral motion by glide is thus possible if material is exchanged between corresponding cells with the same number of atoms, even though the Burgers vector can have a component normal to the grain boundary plane [3, 6–9].

The results presented here cannot address the question of the mechanisms involved in the motion of the dislocation component of the disconnections as it cannot be fully characterized in general grain boundaries and since we do not know the growth directions of each boundary. As such, we cannot correlate the topological characteristics of a boundary with its motion direction. Even in the boundary presented in Fig. 1, in which the growth direction is known, we cannot distinguish between glide and climb, since we expect that the motion of the disconnections will be feasible in both directions where motion in one direction will be preferred (diffusional like motion), and we do not know the kinetic state of the boundary during quenching.

Methodologies for characterization of the dislocation component of disconnections

A variety of methodologies for the characterization of dislocations in grain boundaries exist in the literature. However, these methods are lacking for the case of general grain boundaries, which make up the majority of the population in most materials. Out of the characterized boundaries in the present study, only one case where the structure of the boundary could be determined was encountered. The common approaches for the characterization of dislocations at grain boundaries were applied to this boundary (see supplementary material), but resulted in the inability to describe single dislocations along the boundary. In

the general case, the structure of the boundary cannot be determined, and thus, these methodologies cannot be applied at all. As such, the ability to compare between different grain boundaries was made possible by partial characterization of the projection of the edge component of the dislocations close to normal to the boundary. While this type of characterization is only partial, it is applicable to all general grain boundaries. This method fails only when there is no lattice pattern at all in one of the grains. This can occur in materials with complicated unit cells, or when one of the grains is far from a low-index zone-axis.

In addition to the methods described in the supplementary material for the characterization of the Burgers vector of the dislocation component of disconnections, general grain boundaries can be compared to incoherent phase boundaries due to their low symmetry. Sutton et al. [35] described incoherent phase boundaries according to lattice misfit, as having a spacing between dislocations which are of the order of the dislocation core width [35]. Howe et al. further divided incoherent phase boundaries into three types according to their orientation relationship and the orientation of the habit plane [36]. Applying this terminology to grain boundaries, the boundaries presented in Figs. 3 and 4 fit to the category of an incoherent phase boundary with an irrational (high index) orientation relationship and no rational conjugate habit planes. This type of boundary is characterized as having mismatch between most or all of the atomic planes across the boundary. As such, the boundary has no periodic repetition of a structural unit, and there is overlap between cores of dislocations. In such a boundary, steps are expected to be unnecessary for energy minimization and migration. The boundaries in Figs. 3 and 4 include disconnections with step terms which are not expected to appear according to the classification by Howe et al. [36].

The boundaries presented in Figs. 1, 5, and 6 fit the category of incoherent phase boundaries with an irrational orientation relationship and rational habit planes only in one phase (grain). This type of boundary is characterized by the possibility of some periodic structural repetition at the boundary with large strain resulting in continuous (small) dislocations. This type of interface may have a lower energy than the type mentioned before, mainly due to the reduction in energy correlated with the low-index interface plane. In all of the studied boundaries no periodic structural repetition was noted. In addition, it was not possible to treat the dislocation component of the disconnections as canceling coherency strain due to the lack of repetition of the structure along the boundary, even within short length scales. For example, one might consider the vectors required to connect two matching planes of atoms from both grains using the plane matching approach. These vary along the boundary, such that no similar vectors can be defined.

This approach for describing phase boundaries supports the results presented here, which indicate a low symmetry and a high dislocation density. A high dislocation density is associated with an incoherent phase boundary, and the dislocations can't be discerned by conventional characterization methods and are not taken into account by existing geometrical theories. This is due to the existence of small elementary Burgers vectors, which may overlap, as predicted by Howe et al. for low symmetry phase boundaries.

The anisotropic nature of the dislocation component of the disconnections

While the edge component of the dislocations close to normal to the boundary plane may lay parallel to and originate from many different crystallographic planes, it was found to be aligned mainly parallel to and originate mainly from {100}- and {110}-type planes. The edge component of dislocations which is close to normal to the boundary was parallel to {100} and {110} planes in grains which were oriented close to different zone axes (<100>, <210>, <111>, <211>) and in samples annealed both at 1425 °C and 1350 °C. The planes from the other grain, from which the edge component of the dislocations originated, were mainly {100} and {110} (out of {211}, {100}, {110}). When characterizing the extra planes along a grain boundary plane, the dislocation line is characterized. Since from the micrographs it appears that the dislocation component of the disconnections has at least an edge component, the overall Burgers vector will have a component along the <100> and <110> directions.

The step character of the disconnections found along grain boundaries in $SrTiO_3$ annealed under a relatively high oxygen partial pressure at the same temperatures was found to be mainly parallel to

{100}- and {110}-type planes [12]. This was found regardless of the annealing temperature, cooling rate, and orientation of the delimiting grains, as summarized in Table 2 based on the work detailed in [12]. As can be seen in Table 2, out of the 42 grain boundary and step planes mentioned in the table only two were not {001} or {110} planes. At the same time, the dislocations analyzed here showed preference toward the same crystallographic planes ({110} and {100} planes) as summarized in Table 3, regardless of changes in the annealing temperature, which indicates its anisotropic nature. The preference of the edge component of the dislocations, which is close to normal to the boundary, to be aligned mainly parallel to and to originate mainly from {100}- and {110}-type planes, was less pronounced than the occurrence of the grain boundary and step planes mainly parallel to the {110} and {100} planes. As such, there were more exceptions to this preference in the dislocation analysis rather than in the step term analysis (Tables 3 and 2 accordingly). Extra planes were also found parallel to other planes as well (e.g., {211} and {111} planes). Thus, the edge component of the dislocations, which is close to normal to the boundary, was found to be anisotropic, however less anisotropic than the step character of the disconnections.

The density of the dislocations between steps (meaning along grain boundary plane segments) may also vary. Either very few, several, or many extra planes along segments of the grain boundary plane were noted. The density of the steps is strongly correlated with the curvature of the boundary. In a general boundary, the steps also have a dislocation component, and thus the dislocation density is also assumed to be related to the curvature of the boundary. The orientation of the grains creating the boundary will also affect the dislocation density, since a larger orientation mismatch between the grains will result in more disconnections. Finally, the orientation of the macroscopic grain boundary plane also affects the density of the dislocations. When a macroscopic grain boundary plane is not flat and oriented parallel to a low-index plane, it will evolve into steps and microscopic grain boundary planes which tend to be parallel to low-index planes. In the general case, the steps include a dislocation component. Thus, certain orientations of the macroscopic grain boundary plane will evolve into many disconnections, whereas other will include fewer disconnections.

The existence of the anisotropic edge dislocation component (which is close to normal to the boundary) of disconnections mainly parallel to {001} and {110} planes is correlated with the types of step and grain boundary planes in such boundaries. These were found to be aligned mainly parallel to the same crystallographic planes [12]. The macroscopic grain

Table 2 A summary of the work done to characterize the step component of disconnections at general grain boundaries in $SrTiO_3$ annealed under high oxygen partial pressure [12]

Orientation of one of the delimiting grains	Orientation of grain boundary and step planes	Processing information	Number of characterized boundaries
<100>	{100} and {110}	Annealing temperatures: 1350, 1425, 1550 °C Cooling rate: furnace-cooled and water-quenched	11
<110>	{100} and {110}	Annealing temperatures: 900, 1350, 1425 °C Cooling rate: furnace-cooled, gas-quenched and water-quenched	6
<111>	{101} and {110}	Annealing temperatures: 1350 °C Cooling rate: furnace-cooled and water-quenched	2
<210>	{100} and {112}	Annealing temperatures: 1350 °C Cooling rate: furnace-cooled	1
<211>	{110} and {111}	Annealing temperatures: 1350 °C Cooling rate: gas-quenched	1

The table is sorted according to the orientation of one of the delimiting grains which is close to a low-index zone-axis. Grain boundary and step planes which are not parallel to {001} or {110} planes are marked in red

Table 3 A summary of the results in this work which are related to the orientation of the edge component of the dislocations close to normal to the boundary at general grain boundaries in $SrTiO_3$ annealed under high oxygen partial pressure

Edge component close to normal to the boundary parallel to	Originating from	Processing information	Number of characterized boundaries
{200} planes in a grain close to a <001> zone-axis	{110}	Annealing temperatures: 1350, 1425 °C Cooling rate: furnace-cooled, water-quenched	4
{200} planes in a grain close to a <012> zone-axis	{110} planes in a grain close to a <110> zone-axis	Annealing temperatures: 1350 °C Cooling rate: water-quenched	1
{110} planes in a grain close to a <001> zone-axis	{211}	Annealing temperatures: 1350 °C Cooling rate: furnace-cooled	1
{110} planes in a grain close to a <111> zone-axis	{211}	Annealing temperatures: 1350 °C Cooling rate: water-quenched	1
{110}	{100} planes in a grain close to a <013> zone-axis	Annealing temperatures: 1350 °C Cooling rate: gas-quenched	1
{110} planes in a grain close to a <112> zone-axis	{110}	Annealing temperatures: 1350 °C Cooling rate: gas-quenched	2
{111} planes in a grain close to a <211> zone-axis	{400}	Annealing temperatures: 1350 °C Cooling rate: furnace-cooled	1
{111}	{110} planes in a grain close to a <001> zone-axis	Annealing temperatures: 1550 °C Cooling rate: furnace-cooled	1
{211}	{211} and {210}	Annealing temperatures: 1350 °C Cooling rate: furnace-cooled	2
{310} or {300}	{110} planes in a grain close to a <001> zone-axis	Annealing temperatures: 900, 1350 °C Cooling rate: furnace-cooled, water-quenched	2

The analysis was done based on the plane matching approach. The table is sorted according to the orientation of the extra planes which account for the edge component of the dislocations close to normal to the boundary at the studied boundaries. Extra planes and planes to which they were correlated that are not parallel to {001} or {110} are marked in red

boundary plane was found to be aligned parallel to {001}-type planes, within a range of a few degrees, more than to other planes at different temperatures (1300 °C, 1350 °C, 1400 °C, 1425 °C) using EBSD [37–39]. The macroscopic grain boundary plane was also found to be stepped and thus composed of steps and grain boundary planes which were mainly parallel to {001} and {110} planes [12]. Due to the perovskite structure of $SrTiO_3$, mainly {001} and {110} planes will be normal to the grain boundary and step planes. The curvature of the macroscopic grain boundary plane can be defined by the density of steps. Thus, while the macroscopic grain boundary plane can have a certain orientation, which is affected by the density of the steps, it can be tilted from low-index planes by a few degrees due to the existence of steps, where the step and grain boundary planes remain parallel mainly to {001} and {110} planes. This was noted by large regions of high values of multiplications of random distribution next to {001} planes in the stereographic projections of the grain boundary plane distributions [37, 38]. Thus, while the macroscopic grain boundary plane has a certain orientation, it is composed of grain boundary and step planes mainly parallel to {001} and {110} planes, and as a result is likely to have {001} or {110} planes close to being normal to it. As such mainly {001} and {110} planes will be taken into account in the dislocation analysis described in this work (describing projection of the edge component of the dislocations close to normal to the boundary). Given that the density of the steps defines the deviation of the macroscopic grain boundary plane from the orientation of the microscopic grain boundary plane segments, variations in the amount of steps can increase this deviation, increasing the probability of planes other than {001} and {110} being close to normal to the macroscopic grain boundary plane. This will result in planes other than {001} and {110} being used for the dislocation component analysis, accounting for the dislocation component being less anisotropic than the step component, as was shown in this work.

Dislocations and kinetics

The low symmetry of the boundaries and the dependency of the dislocations on the curvature of the boundary, the orientation of the grains creating the boundary and the orientation of the macroscopic grain boundary plane does not allow us to detect a typical dislocation behavior as a function of annealing temperature, orientation of the grains or the length of the grain boundary plane segments. For example, extra planes parallel to {200} planes in a grain oriented in or close to the <100> zone-axis originating from {110} planes were noted in a polycrystalline sample annealed at 1350 °C and furnace-cooled (Fig. 3), and in diffusion-bonded samples annealed at 1425 °C with either a <110> single crystal (noted twice) or a <001> single crystal (Fig. 2). The orientation of the other grain in all of these cases varied. This indicates that the dislocation nature has no clear correlation with the change in grain boundary mobility in $SrTiO_3$ annealed under a relatively high oxygen partial pressure that was measured elsewhere [15, 16]. This means that similar possibilities for the orientation and density of the edge component of the dislocations which is close to normal to the boundary are available before and after the change in mobility.

Even though a similar nature of the edge dislocation component of the disconnections with a step term was noted, different quantities of several variations of the edge dislocation component can occur at different temperatures, accounting for the change in mobility. Quantifying different types of dislocations requires analysis of many boundaries and is beyond the scope of this work. At the same time, the steps and dislocations act similarly regardless of the annealing temperature and show a clear preference toward {100} and {110} planes. A similar anisotropic behavior of dislocations parallel the {100} and {110} planes was also noted in the literature [31–33, 40]. The change in mobility is suggested to be associated with changes in the chemistry of the boundaries, which will be the topic of a separate publication.

Summary and conclusions

When characterizing the Burgers vector of the dislocation component of the disconnections (as demonstrated in the supplementary material), existing methods used to describe high symmetry boundaries fail to fully characterize the dislocations at general grain boundaries. The proximity of the dislocations and the variety of different types of disconnections prevented the characterization of single disconnections, even if the structure of the boundary can be determined (for a grain boundary where both boundary delimiting crystals are in a low-index zone-axis and the boundary plane is parallel to the incident electron beam). In addition, it was shown that grain boundary dislocations appear along the boundary plane. All types of disconnections were found to be non-uniformly distributed along the boundaries. The inability to fully characterize the structure of general grain boundaries in addition to the lack of knowledge about the kinetic state of the boundaries during quenching resulted in the inability to define the mechanism of motion of the dislocations (climb or glide).

The density of the dislocations between steps (expressed by the number of extra planes along a grain boundary plane segment between steps in the plane matching approach) may also vary. Either very few, several, or many extra planes along a grain boundary plane were noted. The dislocation density is assumed to be related to the curvature of the boundary, the orientation of the grains creating the boundary, and the orientation of the macroscopic grain boundary plane. As such, the density of the dislocations results from the microstructure and doesn't necessarily divide between different types of disconnections.

Using a plane matching approach, the anisotropic nature of the edge component (close to normal to the boundary) of the dislocation character of grain boundary disconnections in $SrTiO_3$ was detected. The disconnections were found to have a dislocation component in all of the studied boundaries, of which the edge component close to normal to the boundary was aligned mainly parallel to {001} and {110} planes. This anisotropic behavior was found to be less anisotropic compared to the step component of these disconnections.

The dislocation nature had no clear correlation with the change in grain boundary mobility in $SrTiO_3$ annealed under a relatively high oxygen partial pressure. Similar possibilities for the orientation and density of the edge component of the dislocations close to normal to the boundary were noted before and after the change in mobility.

Acknowledgements

The authors acknowledge Lothar Houben for assistance with acquiring the data set presented in Figs. 1 and 2 in this manuscript and Fig. S1 and S2 in the supplementary material, and for detailed discussions. The authors thank D. Medlin for his comments on the manuscript and extended discussions. This work was partially supported via a German-Israel Fund (GIF) Grant No. I-1276-401.10/2014.

Electronic supplementary material: The online version of this article (https://doi.org/10.1007/s10853-018-3096-4) contains supplementary material, which is available to authorized users.

Reference

[1] Gleiter H (1969) Mechanism of grain boundary migration. Acta Metall 17:565. https://doi.org/10.1016/0001-6160(69)90115-1

[2] Gleiter H (1969) Theory of grain boundary migration rate. Acta Metall 17:853. https://doi.org/10.1016/0001-6160(69)90105-9

[3] Pond RC, Hirth JP (1994) Defects at surfaces and interfaces. Sol State Phy 47:287–365. https://doi.org/10.1016/S0081-1947(08)60641-4

[4] Khater HA, Serra A, Pond RC, Hirth JP (2012) The disconnection mechanism of coupled migration and shear at grain boundaries. Acta Mater 60:2007. https://doi.org/10.1016/j.actamat.2012.01.001

[5] Hirth JP, Pond RC (1996) Steps, dislocations and disconnections as interface defects relating to structure and phase transformations. Acta Mater 44:4749. https://doi.org/10.1016/S1359-6454(96)00132-2

[6] Pond RC, Ma X, Hirth JP, Mitchell TE (2007) Disconnections in simple and complex structures. Philos Mag 87:5289. https://doi.org/10.1080/14786430701651721

[7] Howe JM, Pond RC, Hirth JP (2009) The role of disconnections in phase transformations. Prog Mater Sci 54:792. https://doi.org/10.1016/j.pmatsci.2009.04.001

[8] Pond RC, Shang P, Cheng TT, Aindow M (2000) Interfacial dislocation mechanism for diffusional phase transformations exhibiting martensitic crystallography: formation of TiAl + Ti_3Al lamellae. Acta Mater 48:1047. https://doi.org/10.1016/S1359-6454(99)00416-4

[9] Pond R, Ma X, Chai Y, Hirth J (2007) Topological modelling of martensitic transformations. Dislocat Solids 13:225

[10] Hirth JP (1994) Dislocations, steps and disconnections at interfaces. J Phys Chem Solids 55:985. https://doi.org/10.1016/0022-3697(94)90118-X

[11] Han J, Thomas SL, Srolovitz DJ (2018) Grain-boundary kinetics: a unified approach. Prog Mater Sci 98:386. https://doi.org/10.1016/j.pmatsci.2018.05.004

[12] Sternlicht H, Rheinheimer W, Hoffmann MJ, Kaplan WD (2016) The mechanism of grain boundary motion in $SrTiO_3$. J Mater Sci 51:467. https://doi.org/10.1007/s10853-015-9058-1

[13] Balluffi RW, Brokman A, King AH (1982) CSL/DSC lattice model for general crystalcrystal boundaries and their line defects. Acta Metall 30:1453. https://doi.org/10.1016/0001-6160(82)90166-3

[14] Howe JM (1997) Interfaces in materials: atomic structure, kinetics and thermodynamics of solid–vapor, solid–liquid and solid–solid interfaces. Wiley, New York

[15] Rheinheimer W, Hoffmann MJ (2015) Non-Arrhenius behavior of grain growth in strontium titanate: New evidence for a structural transition of grain boundaries. Scr Mater 101:68. https://doi.org/10.1016/j.scriptamat.2015.01.021

[16] Rheinheimer W, Bäurer M, Handwerker CA, Blendell JE, Hoffmann MJ (2015) Growth of single crystalline seeds into polycrystalline strontium titanate: anisotropy of the mobility, intrinsic drag effects and kinetic shape of grain boundaries. Acta Mater 95:111. https://doi.org/10.1016/j.actamat.2015.05.019

[17] Baurer M, Kungl H, Hoffmann MJ (2009) Influence of Sr/Ti Stoichiometry on the densification behavior of strontium titanate. J Am Ceram Soc 92:601. https://doi.org/10.1111/j.1551-2916.2008.02920.x

[18] Barthel J, Houben L, and Tillmann K (2015) FEI Titan G3 50-300 PICO. J Large-Scale Res Facil, A34 1. https://doi.org/10.17815/jlsrf-1-57

[19] Baram M, Kaplan WD (2008) Quantitative HRTEM analysis of FIB prepared specimens. J Microsc 232:395. https://doi.org/10.1111/j.1365-2818.2008.02134.x

[20] http://qstem.org/ (2017)

[21] Bishop CM, Cannon RM, Carter WC (2005) A diffuse interface model of interfaces: grain boundaries in silicon nitride. Acta Mater 53:4755. https://doi.org/10.1016/j.actamat.2005.07.008

[22] Yu Z, Muller DA, Silcox J (2004) Study of strain fields at a-Si/c-Si interface. J Appl Phys 95:3362. https://doi.org/10.1063/1.1649463

[23] Huang K (1947) X-Ray reflexions from dilute solid solutions. Proc R Soc Ser A Math Phys Sci 190:102. https://doi.org/10.1098/rspa.1947.0064

[24] Wang ZL (1995) Elastic and inelastic scattering in electron diffraction and imaging. Plenum Press, New York

[25] Klie RF, Browning ND (2000) Atomic scale characterization of oxygen vacancy segregation at $SrTiO_3$ grain boundaries. Appl Phys Lett 77:3737. https://doi.org/10.1063/1.1330572

[26] Browning ND, Pennycook SJ, Chisholm MF, McGibbon MM, McGibbon AJ (1995) Observation of structural units at symmetric [001] tilt boundaries in $SrTiO_3$. Interface Sci 2:397. https://doi.org/10.1007/BF00222626

[27] Browning ND, Buban JP, Moltaji HO, Pennycook SJ, Duscher G, Johnson KD, Rodrigues RP, Dravid VP (1999) The influence of atomic structure on the formation of electrical barriers at grain boundaries in $SrTiO_3$. Appl Phys Lett 74:2638. https://doi.org/10.1063/1.123922

[28] Kim M, Duscher G, Browning ND, Sohlberg K, Pantelides ST, Pennycook SJ (2001) Nonstoichiometry and the electrical activity of grain boundaries in SrTiO3. Phys Rev Lett 86:4056

[29] Sternlicht H, Rheinheimer W, Kim J, Liberti E, Kirkland AI, Hoffmann MJ, and Kaplan WD, Characterization of grain boundary disconnections in $SrTiO_3$ part II: The influence of superimposed disconnections in image analysis. J Mater Sci. https://doi.org/10.1007/s10853-018-3095-5

[30] Du H, Jia C-L, Houben L, Metlenko V, De Souza RA, Waser R, Mayer J (2015) Atomic structure and chemistry of dislocation cores at low-angle tilt grain boundary in $SrTiO_3$ bicrystals. Acta Mater 89:344. https://doi.org/10.1016/j.actamat.2015.02.016

[31] Nishigaki J, Kuroda K, Saka H (1991) Electron microscopy of dislocation structures in $SrTiO_3$ deformed at high temperatures. Phys Status Solidi (a) 128:319. https://doi.org/10.1002/pssa.2211280207

[32] Matsunaga T, Saka H (2000) Transmission electron microscopy of dislocations in $SrTiO_3$. Philos Mag Lett 80:597. https://doi.org/10.1080/09500830050134309

[33] Narayan J, Sharan S, Singh RK, Jagannadham K (1989) Misfit dislocations in superconducting thin films on $SrTiO_3\{010\}$. Mater Sci Eng B 2:333. https://doi.org/10.1016/0921-5107(89)90009-3

[34] Jia C-L, Lentzen M, Urban K (2004) High-resolution transmission electron microscopy using negative spherical aberration. Microsc Microanal 10:174. https://doi.org/10.1017/S1431927604040425

[35] Sutton AP, Balluffi RW (1995) Interfaces in crystalline materials. Clarendon Press, Oxford

[36] Howe JM, Aaronson HI, Hirth JP (2000) Aspects of interphase boundary structure in diffusional phase transformations. Acta Mater 48:3977. https://doi.org/10.1016/S1359-6454(00)00183-X

[37] Rheinheimer W, Bäurer M, Chien H, Rohrer GS, Handwerker CA, Blendell JE, Hoffmann MJ (2015) The equilibrium crystal shape of strontium titanate and its relationship to the grain boundary plane distribution. Acta Mater 82:32. https://doi.org/10.1016/j.actamat.2014.08.065

[38] Saylor DM, El Dasher B, Sano T, Rohrer GS (2004) Distribution of grain boundaries in $SrTiO_3$ as a function of five macroscopic parameters. J Am Ceram Soc 87:670. https://doi.org/10.1111/j.1551-2916.2004.00670.x

[39] Sano T, Saylor DM, Rohrer GS (2003) Surface energy anisotropy of $SrTiO_3$ at 1400 °C in air. J Am Ceram Soc 86(11):1933–1939

[40] Furushima Y, Arakawa Y, Nakamura A, Tochigi E, Matsunaga K (2017) Nonstoichiometric [012] dislocation in strontium titanate. Acta Mater 135:103. https://doi.org/10.1016/j.actamat.2017.06.017